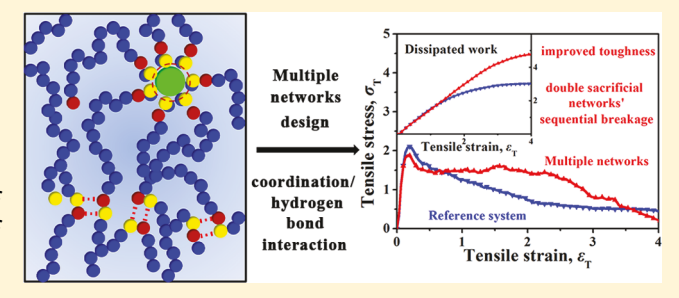
Constructing Sacrificial Multiple Networks To Toughen Elastomer

Zhiyu Zhang,[†] Jun Liu,^{*,†,‡} Sai Li,[†] Ke Gao,[†] Venkat Ganesan,^{*,||} and Liqun Zhang^{†,‡,§}

Supporting Information

ABSTRACT: Designing sacrificial bonds or networks has emerged as a popular strategy to fabricate high-performance elastomeric materials. Herein, we consider the properties of a special kind of double sacrificial multiple networks (MNs), which are composed of one chemically cross-linked covalent network, one noncovalent hydrogen bond network, and one noncovalent coordination network. We examine the effects of the chemical cross-linking density C, the number of coordination beads N_{c} , and the coordination interaction strength ε_c on the structural characteristics of these MNs. The



larger concentration of coordination beads and stronger coordination interactions are shown to result in a larger coordination network which partly replaces the hydrogen bond network. By applying triaxial deformation, we evaluate the toughening mechanism of the MNs and determine the key parameters underlying the toughness of the MNs. In systems with strong coordination interactions, the enhanced toughness is shown to arise from the long and oriented polymer fibers induced by physical cross-linking sites in the coordination network. Furthermore, the characteristic sequential breakage of the different sacrificial networks occurs during deformation, with the hydrogen bond network sacrificed to dissipate energy during the initiation of strain, followed by the coordination network at much larger magnitudes of tensile strain. In general, this simulation study not only demonstrates the toughening mechanism of the double sacrificial networks in MNs under deformation but also provides some guidelines for the fabrication of materials with good mechanical properties via multiple network design.

1. INTRODUCTION

Downloaded by UNIV OF TEXAS AT AUSTIN at 09:56:06:964 on June 06, 2019 from https://pubs.acs.org/doi/10.1021/acs.macromol.9b00116.

Elastomers with high extensibility and excellent recoverability have attracted significant attention in a number of applications, such as tires, shape-memory materials, and shock absorbers. 1-It is well recognized that compounding elastomers with nanoscale fillers serves as a convenient strategy to gain high mechanical strength and toughness. However, the efficiency of such an approach greatly depends on the filler dispersion, the interfacial interaction, and the amount of the fillers added.^{4,5} Meanwhile, to ensure recoverability, introducing cross-links into the elastomeric matrix is needed, which, however, could lead to the formation of stress concentrations during the deformation process.⁶ Therefore, it is still quite challenging to achieve high toughness in covalently cross-linking elastomers.

Experimentally, double networks (DNs) have been proposed as an efficient way to toughen the weak single network, with the underlying mechanism attributed to the gradual rupture of the sacrificial network to effectively dissipate energy.^{7,8} Unlike the permanent covalent bonds of the polymer network, reversible associations, such as those resulting from hydrogen bonds,⁹ metal–ligand coordination bonds,^{10,11} host–guest interactions,¹² and ionic interactions,^{13,14} have been proposed as sacrificial bonds which break and reform to endow the system with better toughness.

Not surprisingly, constructing double or multiple networks (MNs) with different reversible associations has already become a popular strategy to fabricate elastomers with high toughness, strength, and self-healing properties. 15-19 For instance, physical hydrogels consisting of two kinds of ionic bonds with different strengths have been demonstrated to exhibit high toughness.²⁰ In their design, the strong bonds serve as permanent cross-links, while the weak but reversible bonds break first to dissipate energy and then reform. Similarly, hybrid gels constructed by a combination of ionic networks and different covalently cross-linked networks have been shown to also exhibit high stretchability. 21 Introducing reversible hydrogen bond together with dynamic Zn²⁺-triazole coordination into the permanent, covalently linked polymer system has also been successfully explored.^{22'} Similarly, Huang et al. fabricated rubber/graphene composites by introducing sacrificed pyridine-Zn²⁺-catechol coordination at the interface, which successfully increased the overall mechanical properties.²³ A dual physical cross-linking (DPC) strategy combining the coordination bond and hydrogen bond was also shown to lead to hydrogels with ultrahigh strength and

Received: January 16, 2019 Revised: May 10, 2019



Α

[†]Key Laboratory of Beijing City on Preparation and Processing of Novel Polymer Materials, [‡]Beijing Engineering Research Center of Advanced Elastomers, and State Key Laboratory of Organic-Inorganic Composites, Beijing University of Chemical Technology, 100029 Beijing, People's Republic of China

Department of Chemical Engineering, The University of Texas at Austin, Austin, Texas 78712, United States

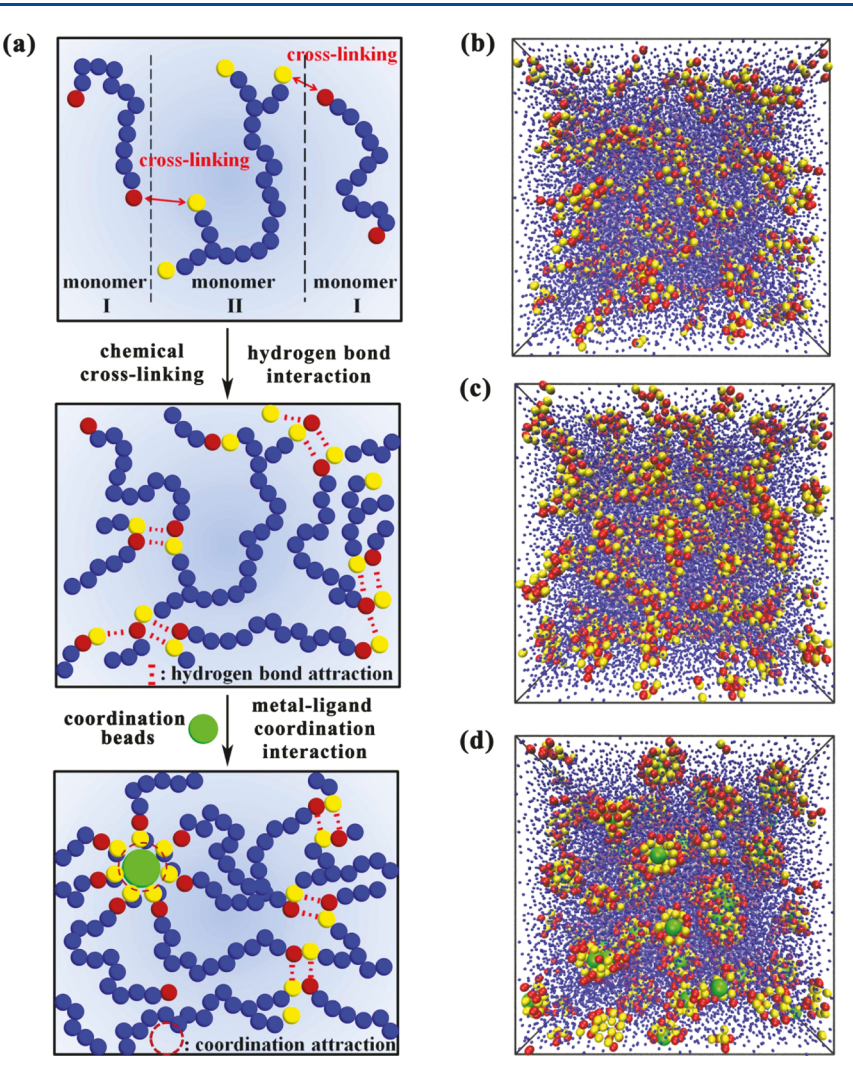


Figure 1. (a) Construction of sacrificial multiple networks: step I forms the chemical network and the resulting hydrogen bonding network, and step II forms the second physical network that models the metal—ligand coordination network. Notably, the blue, red, yellow, and green beads represent the beads in the elastomer backbone, reactive site I, reactive site II, and the coordination bead, respectively. (b) System with low chemical cross-linking density, C = 0.035. Notably, only cross-linked reactive sites are marked with yellow and red. (c) System with high chemical cross-linking density, C = 0.067. (d) Multiple network system C = 0.067, $N_c = 100$, $ε_c = 50.0$, compounded with coordination beads with its number $N_c = 100$, after the chemically cross-linking C = 0.067. Besides the coordination interaction, $ε_c = 50.0ε$ denotes the interaction strength between the reactive site II and the coordination beads.

toughness.²⁴ The use of metal-ligand coordination for toughening the multiple networks was also shown to provide attractive mechanical properties.^{25–27}

In our previous work, we have successfully applied coarsegrained molecular dynamics simulation to mimic several kinds of reversible sacrificial bonds. By introducing a model to study the cooperativity of hydrogen bond and Zn-triazole coordination, we have fabricated and investigated elastomers with enhanced mechanical properties and self-healing capacity. 16 Also, the reversible coordination bond was introduced into the elastomer by a multiphase design, which was shown to substantially enhance the toughness and selfhealing properties.²⁸ With simulations, we have revealed the toughening mechanism of such a multiphase design and elucidated the mechanism of the sacrifice of the reversible network. Furthermore, based on a double-network system, we have investigated the effect of the hydrogen bond interaction strength on the dispersion of physically cross-linking sites as well as the mechanical properties.²

Despite the insights arising from the studies above, it is still unresolved on how to reasonably incorporate multiple noncovalent networks within each other to facilitate enhanced toughness. Besides, to maximize the contribution of the sacrificial bonds to the mechanical properties, an elucidation at the molecular level on the toughening mechanism is also required. The toughening mechanism of the multiple networks (MNs) together with the interplay between coordination interactions and hydrogen bonds has not been fully explored in the past studies. Most research studies about the toughening mechanism in the double network (DN) and triple network systems have attributed the increased toughness to the enhanced resistance against the crack propagation by forming a large damage zone at the crack tip. ^{19,22,30} Although they have observed that the damage zone forms with the breakage of the fragile sacrificial network via high-resolution equipment, such as the three-dimensional violet laser scanning microscope and the atomic force microscope, direct evidence revealing the structural evolution in different kinds of noncovalent networks,

and the approaches to manipulate the mechanical properties on the molecular level are still lacking.

To clearly reveal the toughening mechanism of MNs on the molecular level and exploit some approaches to precisely tune the mechanical properties, we use computer simulations within a coarse-grained model to study the properties of a multiplenetwork (MN) system that incorporates a covalent network, and a combination of weak hydrogen bonds and strong coordination networks to achieve toughening. Based on our previous work, the interaction strength of the hydrogen bond network is fixed at $\varepsilon_h = 5.0\varepsilon$, and we investigate different parameters to elucidate the effect of the coordination network on the structure-property relationship of the whole system. 29,31,32 Specifically, we study the influences of chemical cross-linking density (C), the number of coordination beads (N_c) and the interaction strength of a high-strength coordination network (ε_c) on the morphologies and the mechanical properties of the MNs. By comparing the radial distribution functions (RDFs), we observe that at high interaction strength ε_{σ} an effective coordinated network partly replacing the original hydrogen bond network is formed. Furthermore, with a triaxial deformation testing framework, we evaluate the toughening mechanism of the MNs and determine the key factors underlying the toughness of the MNs probed in our study. Remarkably, the coordination interaction strength is a significant factor in tuning the mechanical properties of the MNs. The sequential breakage of noncovalent networks, the role that the chain orientation plays under deformation, together with the structural evolution of the hydrogen bond network and coordination interaction network are unveiled.

2. MODEL AND METHODS

In our coarse-grained multiple network model inspired by the work of Wu et al., the chemically cross-linked branched polymer is constructed by two different types of repeating units, as shown in Figure 1a. Briefly, all of the repeating units are represented by the standard bead-spring model. Monomer I is modeled as the linear polymer with two reactive sites (reactive site I), which are used to chemically cross-link with the reactive site II (in monomer II) and form the randomly chemically cross-linked network. These reactive site I beads and reactive site II beads are also used to introduce hydrogen bond interactions to the system. Meanwhile, the monomer II is modeled as a branched structure and provides four reactive sites (reactive site II) to achieve the randomly branched structure. As for all monomers, the length of the linear backbone structure is 14, while the branched chain structure of monomer II is 3. The sizes of all polymer beads are identical to the diameter denoted as σ and mass as m. We introduce 1200 monomer I and 600 monomer II into the simulation system, corresponding to the total number of polymer beads for each system of 32 400. Similar to our previous work, the coordination beads are also modeled as the Lennard-Jones (LJ) sphere with the radius equal to 1.0σ , which are introduced to form the coordination network. 16,28 Since the radius of the coordination beads is 2 times that of the polymer bead, the mass of the former is 8 times that of the latter. The density of all beads (including the coordination beads) in the system is set to the same value. Depending on the simulation systems, the number of coordination beads ranges from 0 to 150, and the corresponding mass fraction of the coordination beads varies from 0 to 3.57%.

In our simulations, the interaction of the polymer chain is modeled by the expanded truncated and shifted Lennard-Jones (LJ) potential.³³ To simplify the system, the hydrogen bond interactions and the coordination interactions, are also modeled with this LJ interaction.

$$U_{ij}(r) = \begin{cases} 4\varepsilon_{ij} \left[\left(\frac{\sigma}{r - r_{\text{EV}}} \right)^{12} - \left(\frac{\sigma}{r - r_{\text{EV}}} \right)^{6} \right] - U(r_{\text{cutoff}}), & 0 < r - r_{\text{EV}} < r_{\text{cutoff}} \\ 0, & r - r_{\text{EV}} \ge r_{\text{cutoff}} \end{cases}$$

$$(1)$$

where r_{cutoff} determines the distance $(r - r_{\text{EV}})$, in which the interaction is truncated and shifted so that the energy becomes zero and r is the distance between the two interaction sites of the center of mass. Here, $U(r_{\text{cutoff}})$ is a constant to maintain the continuity of the interaction. The interaction strength between the backbone beads is set to be attractive, $\varepsilon_{\text{non-hydrogen bond}} = 1.0\varepsilon$ and $r_{\text{cutoff}} = 2.5\sigma$. Since the bond lengths of hydrogen bonds (length A_B in A-H···B, 2.2-4.0 Å) and coordination bonds (1.5-3.0 Å) are comparable, we fixed the same cutoff distance $r_{\rm cutoff} = 2.5\sigma$ for all attractive LJ 12-6 interactions and use different interaction strengths. 34-37 According to their different ranges of energy (hydrogen bond: 0.84-168 kJ mol⁻¹; coordination bond: <400 kJ mol⁻¹) and our earlier work about the hydrogen bond, the hydrogen bond interaction strength is fixed at ε_h = 5.0 ε , and the coordination bond interaction has a range ε_c = 10.0 ε - 50.0ε . 29,38,39 It should be noted that when mapping the bead-spring model to real polymers, the energy parameter ε is about 2.5–4.0 kJ mol^{-1} for different polymers, indicating that the value of 5.0ε for the hydrogen bond interaction is about 12.5-20 kJ mol⁻¹, which corresponds to the hydrogen bond with moderate interaction strength for elastomers. 31,40 In our previous work, we showed that when the strength of the nonbonded interaction of the physical network is stronger than 5.0ε , the physical network finally forms via the sufficient associations of the physical cross-linking sites, contributing to an enhancement of the mechanical properties of the system.²⁹ Similarly, the coordination network (as the third network) in the system is also constructed by introducing an attractive interaction between the coordination beads and neighbor reactive site II beads, ε_c and $r_{\rm cutoff}$ = 2.5σ . However, the interaction between the other beads and the coordination beads in the systems is set to be repulsive, $arepsilon_{
m non-coordinate\ bond}=1.0arepsilon$ and $r_{
m cutoff}=1.12\sigma$. The detailed corresponding force field parameters are shown in Table 1.

Table 1. Potential Parameters of the Nonbonded LJ 12-6 Interaction^a

nonbonded pair		$arepsilon_{ m ij}/arepsilon$	$r_{\rm EV}/\sigma$	$r_{ m cutoff}/\sigma$
backbone	backbone	1.0	0	2.5
backbone	reactive site I	1.0	0	2.5
backbone	reactive site II	1.0	0	2.5
backbone	coordination bead	1.0	0.5	1.12
reactive site I	reactive site I	1.0	0	2.5
reactive site I	reactive site II	5.0	0	2.5
reactive site I	coordination bead	1.0	0.5	1.12
reactive site II	reactive site II	1.0	0	2.5
reactive site II	coordination bead	50.0	0.5	2.5
coordination bead	coordination bead	1.0	1.0	1.12

^aIn our simulations, the interaction strength between the reactive site II and coordination bead is a variable.

The bond stretching energy between the adjacent beads is modeled via the stiff finite extensible nonlinear elastic (FENE) potential 31,33

$$E_{\text{bond}}(r) = -0.5kR_0^2 \ln \left(1 - \frac{r}{R_0}\right)^2$$
 (2)

where k is the stiff constant, r is the current bond length, and R_0 is the equilibrium bond length. To simplify the simulation, k and R_0 in all kinds of covalent bonds are set to $30\varepsilon/\sigma^2$ and 1.5σ , respectively.

Initially, all simulations start from a nonoverlapped configuration of two different types of repeating units in a large simulation box. Periodic boundary conditions in three directions are also employed in the simulations. Then, we use the normal pressure and temperature (NPT) ensemble to equilibrate all systems, by adjusting the Nosé—

Hoover temperature thermostat and pressure barostat, $T^*=1.0$ and $P^*=1.0$, and the resulting reduced number density of polymer is determined to be $\rho^*=0.95$, corresponding to the density of polymer melt. To further confirm the melt state of the system, we determine the glass-transition temperature, by calibrating volume—temperature curves and using the linear fitting to obtain the glass-transition temperature. The $T_{\rm g}$ for the MN systems is shown in Figure S1 and is lower than the temperature chosen for our study. The velocity-Verlet algorithm is used to integrate equations of motion to describe the motion of all beads with the time unit $\delta t^*=0.001$ reduced by the LJ time (τ) . The obtained structure is further equilibrated under the NPT ensemble to ensure that each monomer backbone has moved at least $2R_{\rm g}$ ($R_{\rm g}$ is root-mean-squared radius of gyration of the polymer).

We construct the MN system by following two steps. First, we implement the cross-linking of the randomly branched network, where the chemical cross-linking sites are introduced during a continuous and controllable cross-linking process. Simultaneously, the hydrogen bond interaction is also introduced by turning on the interaction ($\varepsilon_h = 5.0\varepsilon$) between the reactive sites I and II (Figure 1a). The permanent cross-linking bonds are imposed in the noncrosslinked system by randomly selecting and tethering a reactive site I bead from monomer I and a reactive site II bead from monomer II. The cross-linking process is dynamic and continuous, which is affected every 100 time steps. If the distance between these two beads is smaller than 1.0σ , a bond modeled by the FENE potential is produced between these two beads. A similar algorithm has been employed by Kroll et al., except that their cutoff distance was set to be 1.3σ and a probability of 10% to form the cross-linking bond. 44 Since it is not our aim to study a specific cross-linking or vulcanization process, we merely build the cross-linked network, and do not invoke a probabilistic approach. The density of the cross-linking (conversion of the cross-linking reaction) is regulated by the time of the crosslinking process. In our systems, we define the density of cross-linking as $C = N(t)/V^*$, where the reduced volume is $V^* = 34\,000$ and N(t)represents the number of the cross-linking bonds that have been produced at the current time, t. A visualized comparison between low and high cross-linking density can be found in Figure 1b,c. Therein, the C = 0.035 and 0.067 represent that 50 and 95% of the two kinds of monomers have been cross-linked separately. The dependence of the cross-linking rate of the network on temperature and the coarsegrained cross-linking kinetics have been reported in our previous work.²⁹ More discussion about the cross-linking method can be found in the Supporting Information.

Subsequent to the above steps, the coordination network is constructed by introducing the coordination beads with a strong attractive interaction $\varepsilon_c=50.0\varepsilon$ between themselves and reactive site II beads (Figure 1a). Notably, the chemical cross-linking density (C), the number of coordination beads (N_c), and the strength of the coordination interaction (ε_c) can be regulated in the whole process. The obtained final structure is further equilibrated under the NPT ensemble to make sure that each monomer has moved at least $2R_g$. As Figure 1 indicates, the MN system is seen to involve a combination of (i) covalent bonding by cross-linking, (ii) hydrogen bond interaction, and (iii) coordination interaction. For instance, a snapshot introducing the system C=0.067, $N_c=100$, $\varepsilon_c=50.0$ is presented in Figure 1d.

After sufficient equilibrium, the triaxial tensile deformation of multiple networks is performed by following the procedure introduced in our previous work. The triaxial tensile test is generally used to investigate the toughness of the elastomers, which can induce cavitations, crazing, and fracture of the polymer. We can integrate the triaxial stress—strain curve to obtain the dissipated work so as to quantitatively compare the toughening effects. To achieve triaxial deformation, we perform our tensile tests by stretching the simulation box along the Z direction at a constant velocity while keeping the box length unchanged in the other two directions and maintaining the periodic boundary conditions in all directions. The stress $\sigma_{\rm T}$ in the Z direction is represented by the deviatoric tensor, $\sigma_{\rm T} = -P_{zz}$, the hydrostatic pressure in the Z direction. Meanwhile, the

tensile strain $\varepsilon_{\rm T}$ at time t is $(L_z(t)-L_z(0))\cdot L_z(0)^{-1}$, and the tensile rate is set to be $\dot{\varepsilon}_{\rm T}=0.0327/\tau$, which is the same as the simulation work form Gao et al. 52,53 In addition, the second-order Legendre polynomial is used to characterize the chain orientation, $\langle P_2(\cos\theta)\rangle=(3\langle\cos^2\theta\rangle-1)/2$, where θ denotes the angle between the given bond and the deformation direction. 54 The possible value of $\langle P_2(\cos\theta)\rangle$ ranges from -0.5 to 1, and the values -0.5, 1, and 0 indicate a perfect orientation perpendicular to the deformation direction, parallel to the deformation direction, and random orientation, respectively. All of the simulations are carried out using the large scale atomic/molecular massively parallel simulator (LAMMPS), developed by the Sandia National Laboratories. 55 More details of the simulation techniques can be found in our previous work. $^{56-58}$

3. RESULTS AND DISCUSSION

3.1. Structure and Morphology of the Multiple Networks. Before we study the toughening behavior of the MNs, we investigate the structure of the MNs arising from the introduced coordination beads. In view of the fact that coordination interactions manifest only between the reactive site II beads (on monomer II) and the coordination beads, the introduction of the coordination beads interferes with the hydrogen bond network. We begin by briefly discussing the effect of the coordination interaction strength (ε_c) and the number of coordination beads (N_c) on the morphology and structure of the multiple networks.

First, we fix the cross-linking density of following systems and consider the system with no coordination bead $(N_c = 0)$ as the reference system, which only consists of the covalent network and the hydrogen bond network ($\varepsilon_h = 5.0\varepsilon$). The radial distribution functions (RDFs) of the cross-linked reactive site II beads for systems with low (C = 0.035) and high (C = 0.067) cross-linking densities are shown in Figure 2a,b for different ε_c . The peak located at approximately r = 1.05σ represents the beads on the surface of the coordination beads, and the peak at $r = 3.0\sigma$ represents the direct contact on the surface of the coordination beads. From the results displayed in Figure 2a, with an increase in the strength of the coordination interaction (ε_c) beyond ε_c = 10.0, we observe that the reactive site II beads begin to aggregate on the surface of the coordination bead $(r = 1.05\sigma)$ as evidenced by the sharp peak in the RDFs. Such results indicate that the coordination network forms, which consists of the noncovalent cross-linking sites by aggregating the polymer backbones and partly replaces the original hydrogen bond network. Similar results can also be found in the case with high cross-linking density (Figure 2b). Such results indicate that the interaction strength ε_c is of significance for the formation of the coordination network. To confirm the role of high $\varepsilon_{\rm c}$ in the formation of the coordination network, a comparison between the RDFs of the systems with different N_c is shown in Figure 2c, where a relatively high chemical cross-linking density (C = 0.067) and a high interaction strength ($\varepsilon_c = 50.0\varepsilon$) are adopted. As is expected, all coordination bead filling systems exhibit the characteristic peaks $(r \approx 1.0\sigma \text{ and } 3.0\sigma)$, in which case the coordination network has formed with such a high interaction strength.

To quantitatively describe the surface aggregation state, i.e., the physical cross-linking sites induced by the coordination interaction, the average number of neighbor cross-linked reactive site II beads around each coordination bead is calculated and shown in Figure 3a. The beads are considered to be "neighbors" if they are within the distance of $r = r_{\rm cutoff} + r_{\rm EV}$, the upper distance limit of the LJ interaction (Figure S2). ⁵⁹ As shown in Figure 3a, independent of the number of

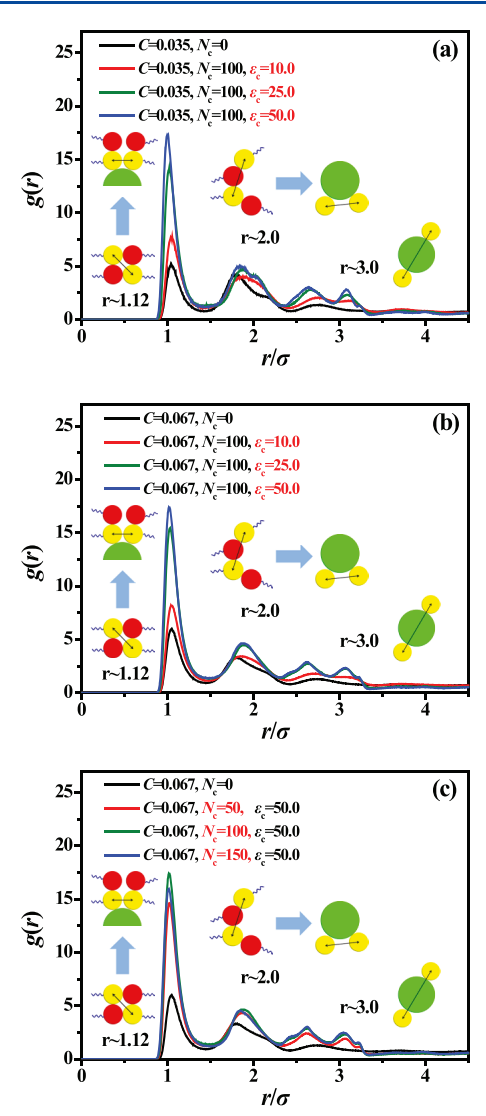
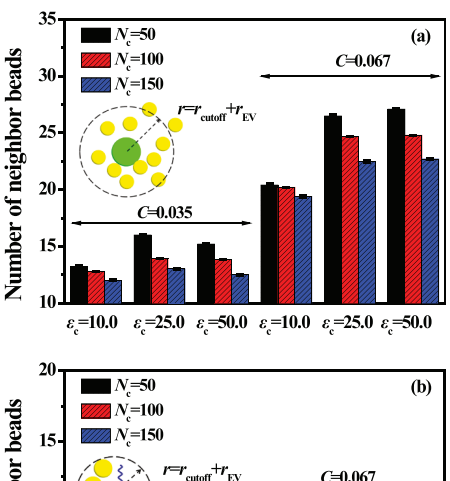


Figure 2. Comparison of the cross-linked reactive site bead II-reactive bead II radial distribution functions, g(r), for systems with different chemical cross-linking densities: (a) low chemical cross-linking density C=0.067. The number of coordination beads, N_c , is fixed at 100 for all systems. (c) Comparison of RDFs for the systems with the different number of coordination beads introduced. The chemical cross-linking density is fixed at C=0.067 and the interaction strength for the coordination interaction is fixed at $\varepsilon_c=50.0\varepsilon$.

coordination beads (N_c) and cross-linking density (C), when the interaction strength (ε_c) changes from 10.0ε to 25.0ε , the average number of neighbor beads practically reaches its asymptotic limit. Notably, only those reactive site II beads which have been bonded with reactive site I beads are involved in this calculation, so the "neighbor" number increases with increasing the cross-linking density. A higher interaction strength denotes a more favorable surface aggregation of the cross-linked reactive site II beads, in which case the formed metal-ligand like structures serve as the noncovalent crosslinking sites, help construct the coordination interaction network, however, inevitably destroy part of the hydrogen bond network. Besides, independent of the interaction strength (ε_c) and cross-linking density (C), neighbor number decreases with increasing the number of coordination beads (N_c) , which is attributed to the fixed total number of cross-linked reactive



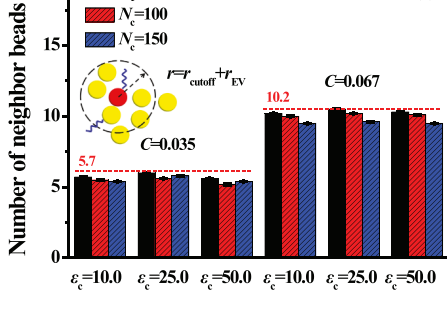


Figure 3. Average number of neighbor cross-linked reactive site II beads around (a) each coordination bead and (b) each reactive site I beads. Notably, the distance limit is $r = r_{\rm cutoff} + r_{\rm EV}$. The red dashed lines represent the neighbor number when $N_{\rm c} = 0$.

site II. In either case, when the interaction strength $\varepsilon_{\rm c}$ increases to 25.0ε , the neighbor number reaches its asymptotic limit. Therefore, combining Figure 2c, a conclusion can be deduced that the morphology of MNs shows less dependence on the number of coordination beads. Furthermore, the neighbor number of each reactive site I bead (Figure 3b) is seen to be almost independent of the interaction strength ($\varepsilon_{\rm c}$) and the number of coordination beads ($N_{\rm c}$). Compared with the systems with $N_{\rm c}=0$ (red dashed lines), only a small decrease in the neighbor number can be found when the interaction strength increases, which indicates that only a small number of hydrogen bond cross-links have been replaced by the coordination bond cross-links.

3.2. Mechanical Properties of the Multiple Networks. Having qualified the effects of coordination interaction strength (ε_c) and the number of coordination beads (N_c) on the structure of multiple networks, we now discuss the results for mechanical properties. We discuss the influence of three parameters separately: the number of coordination beads (N_c) , the coordination interaction strength (ε_c) , and the chemical cross-linking density (C).

3.2.1. Effects of the Number of Coordination Beads. In line with our previous work, the non-constant volume stretching process is generally adopted to simulate the fracture of materials. ^{46,47} To investigate the effect of the number of coordination beads (N_c) , we consider systems in which C=0.035 and $\varepsilon_c=50.0\varepsilon$. The latter choice was motivated by our RDFs results (Figure 2c), which indicated that for $\varepsilon_c=50.0\varepsilon$, a favorable coordination network likely contributes to a good toughness performance result. For our results, the number of coordination beads is varied in the range of 0, 50, 100, and 150, corresponding to the mass fractions of $\phi=0$, 1.22, 2.41, and 3.37%. To quantitatively characterize the toughening effect, we integrate the triaxial stress values to obtain the

dissipated work by following Gersappe et al.,⁴⁹ and such results are displayed in Figure 4.

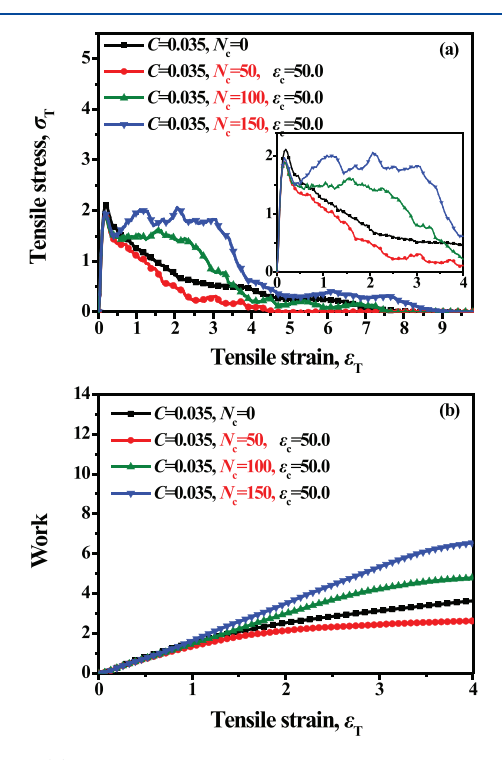


Figure 4. (a) Stress—strain curves for the different number of coordination beads N_c . (b) Dissipated work obtained by integrating the stress—strain curves.

In the tensile stress-strain curves shown in Figure 4a, all systems exhibit a linearly elastic response at small strain and then reach the yielding point, which signifies the onset of voids and cavities. However, compared to the system with $N_c = 0$, a much faster decrease in the tensile stress occurs in the system with $N_c = 50$ after reaching the yielding point and thus results in low mechanical properties. Explicitly, for $N_c = 50$, despite the high strength of ε_c , the combination of the coordination and hydrogen bond network exhibits the lowest dissipated work, indicating an untoughened effect. These features are more clearly seen in Figure 4b, in which the case for $N_c = 50$ is seen to underperform relative to $N_c = 0$. In contrast, systems N_c = 100 and 150 exhibit a much longer stress plateau (Figure 4a) and more dissipated work (Figure 4b), which indicates a much better toughening effect by the appropriate number of coordination beads. Notably, compared with the system with $N_c = 0$, the reduced yielding stress can be found in every compounded system $(N_c \neq 0)$. Previous studies have extensively explored the mechanism affecting the yielding stress: the yielding behavior is found to be controlled by the local interfacial interaction. 49,50 Meng et al. reported that compared with the pure polymer matrix, the repulsive interaction between nanoparticles and polymer induces a decrease in the yielding stress. 50 In our work, the coordination beads possess attractive interactions with reactive site II beads but involve repulsive interactions with the backbone beads. In the system with $N_c = 0$, the hydrogen bond cross-links consist of reactive site I beads and reactive site II beads, being attractive with the backbone beads, which induces high yielding stress. Compared with the unfilled systems with N_c = 0, although in the systems with $N_c \neq 0$ the noncovalent

coordination bond cross-links form via the strong attraction between coordination beads and reactive site II beads, the repulsive interaction between coordination beads and backbone beads induces a decrease in the yielding stress.

To investigate the toughening mechanism, we present the results for the polymer chain orientation in Figure 5a. The trends seen therein, especially the dependence on N_c , are in good agreement with their corresponding tensile stress-strain curves (Figure 4a). Compared with the system $N_c = 0$, systems $N_c = 100$ and 150 also show a longer and higher orientation plateau when the strain is greater than 1.0. Such results indicate that the toughening effect can be attributed to the orientation of the polymer chains induced by the physical cross-linking sites in the coordination network. To provide a more visualized depiction of the mechanism, snapshots of the strain process are displayed in Figure 5b,d. Compared with the system with $N_c = 0$ (Figure 5b), in the system with $N_c = 50$ (Figure 5c) whose chain orientation is the lowest, the voids and cavities emerge and then converge quickly, leading to several single and short fibrils, and finally results in no plateau stress and a clear fracture behavior at large strain. In contrast, a much longer tensile stress plateau occurs when a larger number of coordination beads are introduced to the system ($N_c = 150$, Figure 4a), in which case sufficient coordination beads act as the physical cross-linking sites and initiate long and highly oriented polymer chains/fibrils. Meanwhile, as Figure 5d shows, the oriented polymer chains/fibrils also prevent the cavitations and voids from growing and propagating quickly to sustain the external stress.

To further reveal the molecular changes, except for the chain orientation, we computed the contributions to the total nonbonded interaction energy arising from the coordination and hydrogen bond interactions, respectively (Figure 6a,b). In Figure 6a, it is seen that when compared with other MN systems with coordination beads, the energy of coordination interaction of systems with $N_c = 50$ exhibits a much lower value and is nearly unmodified during the deformation process. Notably, even though the absolute value of energy of system $N_{\rm c}$ = 100 and 150 exhibits a plateau in the initial portion of the strain, a latter decreasing trend is clearly seen and indicates the influence of the coordination interaction to meet the demand of sacrificial network to toughen the MNs. Also, the ΔE_c (ΔE_c = $E_c(\varepsilon_T = 4.0) - E_c(\varepsilon_T = 0)$, the ability to dissipate the energy, shows enormous difference when the N_c increases from 50 to 150, which indicates that the more noncovalent crosslinks compounded in MNs, the more energy will the coordination interaction help to dissipate. Meanwhile, according to the energy of hydrogen bond interaction in Figure 6b, the absolute value of energy also decreases and the hydrogen bond network has been broken to dissipate the energy. Additionally, in Figure 6b, compared with all MNs with $N_c \neq 0$, the hydrogen bond network of the system $N_c = 0$ obviously dissipates the maximum value of ΔE_h ($\Delta E_h = E_h(\varepsilon_T)$ = 4.0) – $E_h(\varepsilon_T = 0)$), the ability to dissipate the energy (Figure S3) during deformation, which also validates that the hydrogen bond network has been interfered by the coordination network when compounding with coordination beads. To support the results of the variations of energy, the variations of the average number of neighbor cross-linked reactive site II beads are shown in Figure 6c, which are also in good agreement with the trends exhibited by the coordination interaction energy (Figure 6a). Meanwhile, different from the staged decreasing trend displayed by the coordination interaction energy, the energy of

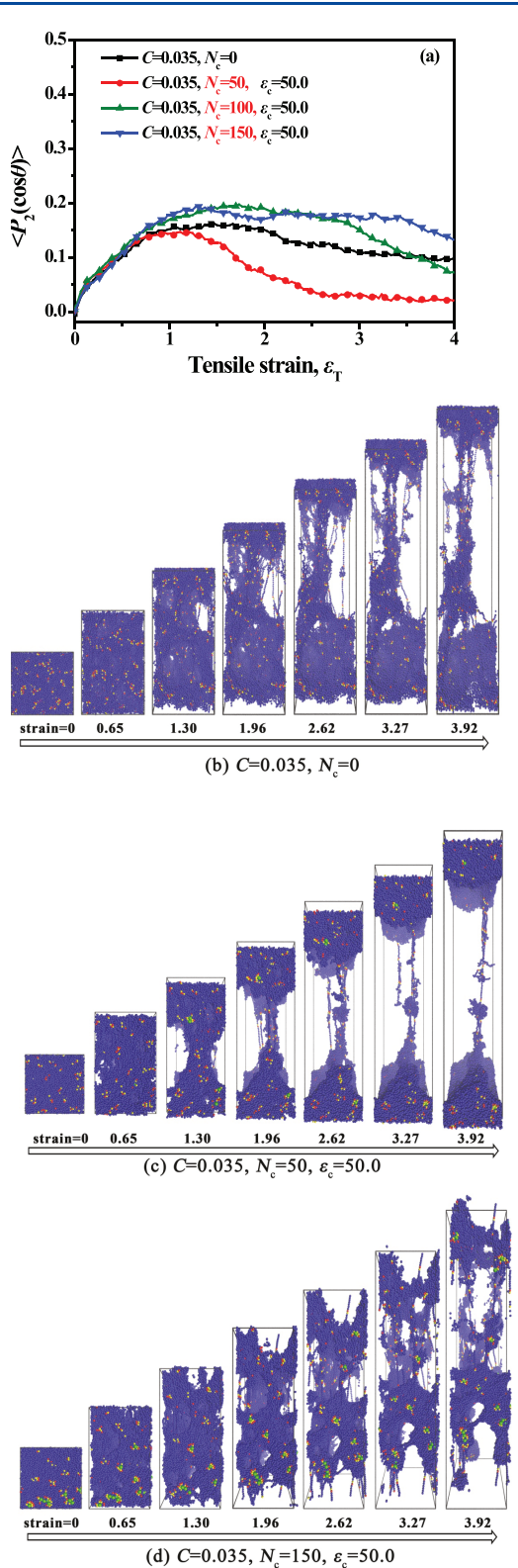


Figure 5. (a) Chain orientation of systems with the different number of coordination beads N_c , which is corresponding to Figure 4a. Snapshots of the systems (b) C = 0.035, $N_c = 0$, (c) C = 0.035, $N_c = 50$, $\varepsilon_c = 50.0$, and (d) C = 0.035, $N_c = 150$, $\varepsilon_c = 50.0$ showing the deformation state at different strains.

hydrogen bond interactions shows a direct and rapidly decreasing trend (Figure 6b), a behavior which is consistent with the variation of neighbor number during deformation

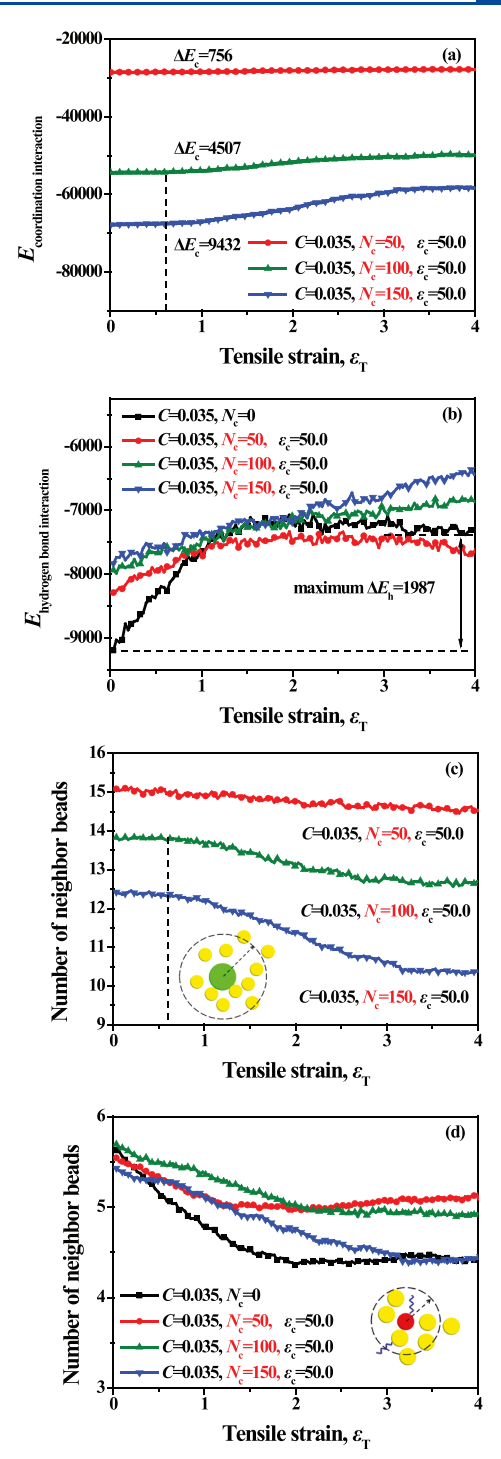


Figure 6. Variations of energy and structural evolutions of noncovalent cross-links. The total (a) coordination interaction energy and (b) hydrogen bond interaction energy as a function of strain during the tensile process. The average number of neighbor cross-linked reactive site II beads around each (c) coordination bead and (d) reactive site I bead. The ΔE for the coordination interaction and hydrogen bond interaction is calculated by $\Delta E = E(\varepsilon_{\rm T} = 4.0) - E(\varepsilon_{\rm T} = 0)$

(Figure 6d). Combining these phenomena about the variation of energy and structural evolution in the toughened MNs (N_c = 100 and 150), the sequential breaking of different noncovalent associations can be deduced: the hydrogen bond cross-links break at the initial strain to dissipate the energy,

while the coordination cross-links do not break until the strain reach around 0.6. The sequential breakage of MNs is proposed as shown in Figure 7.

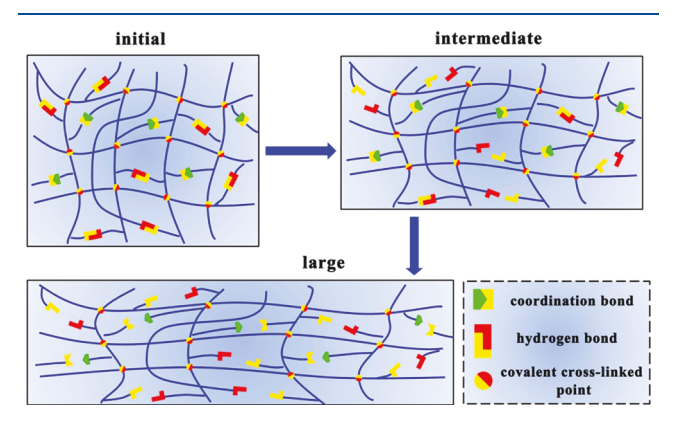


Figure 7. Proposed sequential breakage in multiple networks systems under deformation.

For the low cross-linking density system, introducing sufficient coordination beads not only helps in forming noncovalent coordination cross-links that induce the chain orientation to toughen the MNs, but also helps dissipating much more energy via the breakage of the noncovalent coordination cross-links, and especially, the systems with sufficient coordination cross-links ($N_c = 100$ and 150) show sequential breakage of different noncovalent associations. However, for system with $N_c = 50$, although the coordination interaction is strong enough and has contributed more energy (absolute value of E_c) than that of the hydrogen bond interaction (absolute value of E_h), the noncovalent coordination cross-links are insufficient to induce enough chain orientation to sustain the external stress, and lead to lower mechanical properties than the other systems. In our simulations, the variations of energy, together with the corresponding neighbor numbers are merely used to reflect the structural evolutions of different noncovalent cross-links. The mechanical responses of the MNs are mainly governed by the chain orientation.

To sum up, combining Figures 4–6, the enhanced toughness of MNs is attributed to the long and highly oriented polymer chains/fibrils induced by noncovalent cross-linking sites. Meanwhile, the oriented polymer chains also help in further dissipating the energy with the sequential breakage of the double sacrificial noncovalent networks. Also, these results together demonstrate that to toughen the polymer network by MNs, the effective number of physical cross-linking sites should be considered carefully in formulating such materials.

3.2.2. Effects of the Coordination Interaction Strength and Cross-linking Density. Having investigated the effects of the number of coordination bonds on the MNs, we now present the results for the effects of the coordination interaction strength (ε_c). We divide the following results into two parts: low (C=0.035) and high (C=0.067) chemical cross-linking density. We fix all of the following systems with $N_c=100$. For systems with low (C=0.035) chemical cross-linking density, the strain—stress curves of the systems with ε_c varying from 10.0ε to 50.0ε are shown in Figure 8a. Meanwhile, the dissipated work and the corresponding chain orientation are shown in Figure 8b,c, respectively. The system with $\varepsilon_c=10.0\varepsilon$ shows the lowest tensile stress during the

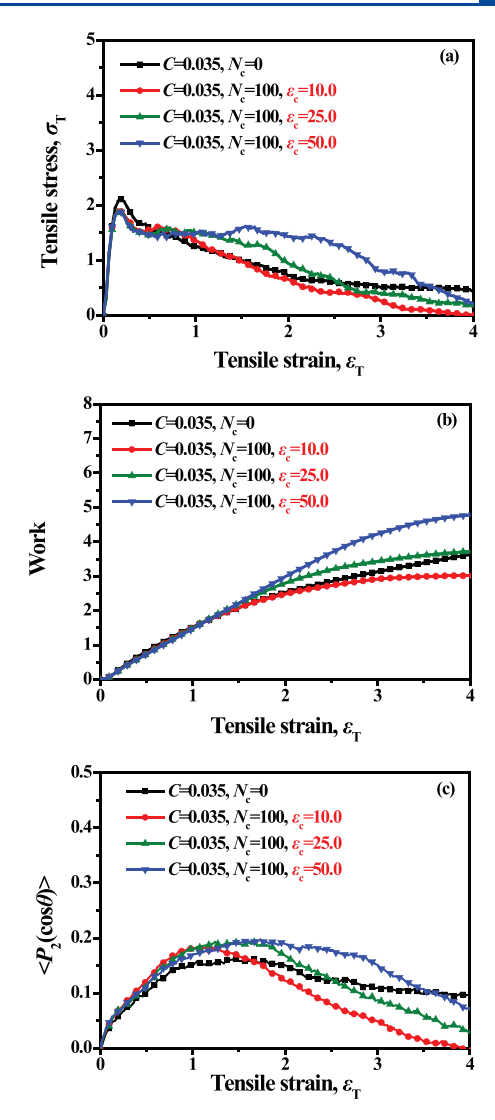


Figure 8. (a) Stress—strain curves for different coordination interaction strengths ε_c . (b) Dissipated work obtained by integrating the stress—strain curves. (c) Chain orientation of systems corresponding to the stress—strain curves.

whole process and its chain orientation also decreases to zero rapidly. Furthermore, according to Figure 8b, it is observed that the coordination beads introduced fail to toughen the multiple networks when $\varepsilon_c = 10.0\varepsilon$ for the presented lowest dissipated work. We recall this for such interaction strength, the RDFs and neighbor numbers results (Figures 2b and 3a) indicate that a coordination interaction network consisting of incomplete coordination cross-links is present, albeit only partly replacing the hydrogen bond network. Although the chain orientation of systems $\varepsilon_{\rm c}$ = 50.0 ε and 25.0 ε shows a decreased trend ($\varepsilon_T > 2.0$), which corresponds to the decrease of the stress, we still consider them to exhibit comparable and enhanced toughness with a much longer and higher stress plateau and more dissipated work compared to the system N_c = 0. Therefore, with an increase in the interaction strength from 10.0ε to 50.0ε , both the plateau tensile stress, the length of the stress plateau, and the dissipated work exhibit the enhanced trend. We conclude that compared with the reference system (C = 0.035, $N_c = 0$), the coordination network in MNs with $\varepsilon_c = 50.0\varepsilon$ and 25.0ε has successfully toughened the elastomers with much more dissipated work.

Besides, they exhibit a much longer and higher tensile stress plateau (0.5 < $\varepsilon_{\rm T}$ < 1.5, when $\varepsilon_{\rm c}$ = 25.0 ε and 0.5 < $\varepsilon_{\rm T}$ < 2.5, when $\varepsilon_{\rm c}$ = 50.0 ε). To sum up, compared with the system with no coordination network, the system with coordination beads exhibits comparable dissipated work when $\varepsilon_{\rm c}$ = 25.0 ε (62.5–100 kJ mol⁻¹), which confirms a threshold of $\varepsilon_{\rm c}$ for tuning the interaction strength and designing the MNs in practice.

Also, the variations in the energy of coordination interaction and hydrogen bond interaction during deformation are displayed, respectively, in Figure 9a,b. Therein, according to their different variation trends, the sequential breakage of different noncovalent cross-links can be found when $\varepsilon_c = 25.0\varepsilon$ and 50.0 ε , but it is seen to disappear when ε_c is set to 10.0 ε . Compared with the characteristic staged decrease in the absolute value of coordination interaction energy in the systems with $\varepsilon_{\rm c}=25.0\varepsilon$ and 50.0ε , the monotonically decreasing trend of energy, the much lower absolute values and the lowest ΔE_c in system $\varepsilon_c = 10.0\varepsilon$ demonstrate that the coordination network dissipates less work and finally fails to effectively toughen the MNs. Such results are further validated by the average number of neighbor cross-linked reactive site II beads (Figure 9c,d). For the neighbor numbers representing different associations, both their decreasing trends and values fit the corresponding variation of energy of interaction. Notably, in the system with $\varepsilon_c = 10.0\varepsilon$, the neighbor number of two kinds of noncovalent associations decreases rapidly with the initiation of strain. Together, these results in Figures 8 and 9 demonstrate that the formation of effective coordination network requires a strong enough ε_c . For the toughened MNs by strong coordination interaction ($\varepsilon_c \ge 25.0\varepsilon$), the oriented polymer chains are still found to be the toughening mechanism, which is same as the former discussion about the number of coordination beads. When weak and incomplete coordination network ($\varepsilon_{\rm c} \geq 10.0\varepsilon$) is introduced into the systems, it interferes and then partly replaces the present toughening network constructed by hydrogen bond interaction $(\varepsilon_h \geq 5.0\varepsilon)$. Although both of the noncovalent cross-links have been sacrificed to dissipate the work, neither of them can initiate enough oriented polymer chains to toughen the elastomers efficiently. Also, with an increase in the ε_c , the sequential breakage of the different kinds of noncovalent associations is found.

The results for systems with C = 0.067 are also probed to verify the influence of $\varepsilon_{\rm c}$ on the toughening effect. From the results displayed in Figure 10a, in comparison with the reference systems with $N_{\rm c}$ = 0, systems with $\varepsilon_{\rm c}$ = 25.0 ε and 50.0ε are seen to exhibit much higher tensile stress and a longer stress plateau, which is consistent with the observation in the systems with low cross-linking density. Also, similar to the former results, system with $\varepsilon_c = 10.0\varepsilon$ shows the lowest tensile stress, whose coordination cross-links are assumed to be not strong enough to sustain the stress. According to the dissipated work in Figure 10b, it finally exhibits decreased toughness compared with $N_{\rm c}$ = 0. After the initial strain ($\varepsilon_{\rm T}$ > 0.6), compared with the reference system with $N_c = 0$, the coordination network effectively toughens the systems for all cases, except when $\varepsilon_{\rm c}$ = 10.0 ε . Furthermore, we observe that there is a rapid enhancement in the tensile stress for the system $\varepsilon_{\rm c} = 50.0\varepsilon$, whose tensile stress quickly increases after its yielding point. In Figure 10c, the chain orientation is enhanced when ε_c increases from 10.0ε to 50.0ε , which fits the stress– strain curves well. However, the differences between the values of orientation are much smaller than those in the former

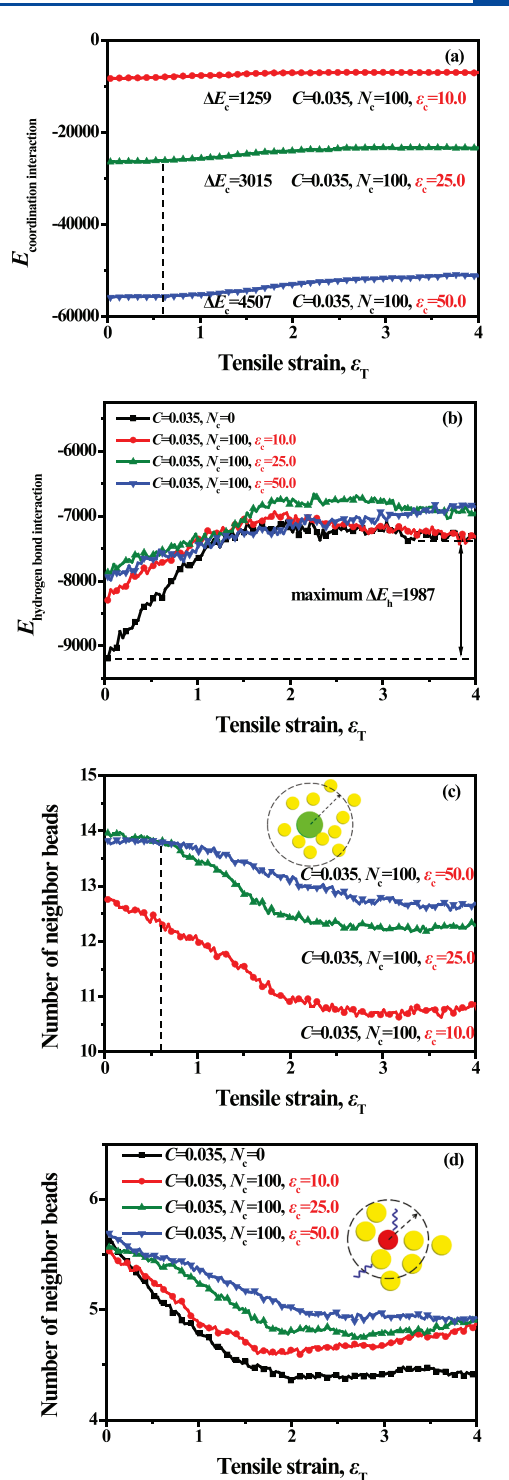


Figure 9. Variations of energy and structural evolutions of noncovalent cross-links. The total (a) coordination interaction energy and (b) hydrogen bond interaction energy as a function of strain corresponding to the tensile process in **Figure 8a**. The average number of neighbor cross-linked reactive site II beads around each (c) coordination bead and (d) reactive site I bead. The ΔE for the coordination interaction and hydrogen bond interaction is calculated by $\Delta E = E(\varepsilon_{\rm T} = 4.0) - E(\varepsilon_{\rm T} = 0)$.

systems with C = 0.035. Notably, a high cross-linking density will greatly enhance the chain orientation, which screens the chain orientation contributed by the noncovalent cross-links (Figure S4). We observe that the orientation of the system

I

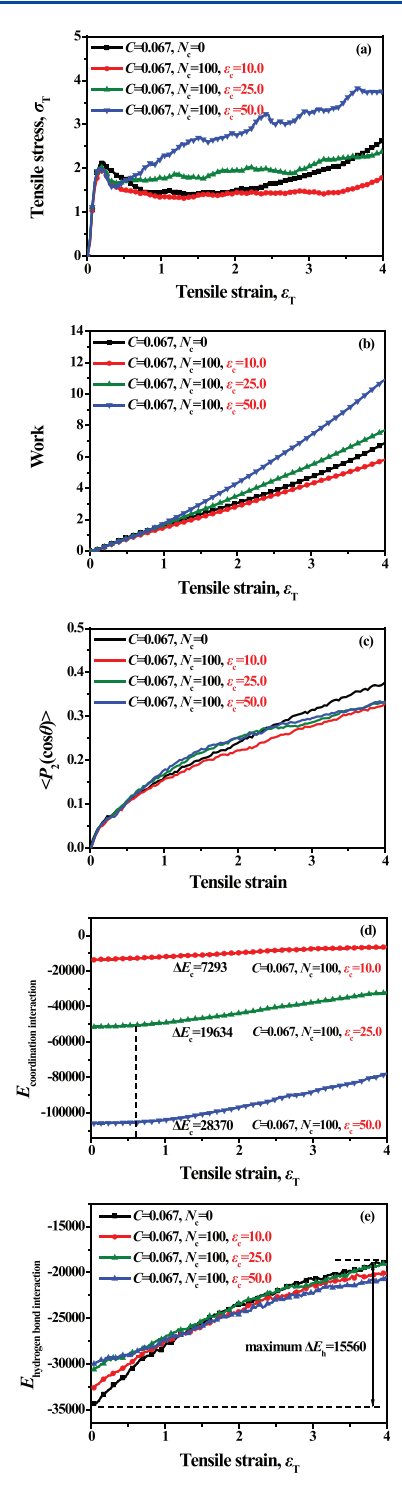


Figure 10. (a) Stress—strain curves for different coordination interaction strength ε_{o} when the chemical cross-linking density C=0.067. (b) Dissipated work obtained by integrating the stress—strain curves. (c) Chain orientation of systems corresponding to the stress—strain curves. The total (d) coordination interaction energy and (e) hydrogen bond interaction energy as a function of strain during the tensile process.

with $N_c = 0$ becomes a bit higher than all MN systems with $N_c \neq 0$ when the strain is greater than 2.5, but the corresponding value of the tensile stress is a little bit smaller than those of the systems with $\varepsilon_c = 25.0\varepsilon$ and 50.0ε . Since the bond orientation is greatly enhanced by many covalent cross-links, which

screens the contributions from the noncovalent cross-links, it is difficult to confirm that the toughening effect completely comes from the increased chain orientation. Here, we just confirm the former observation and conclude that the dissipated work, i.e., the toughening effect, can be greatly enhanced by the high interaction strength ($\varepsilon_c \geq 25.0\varepsilon$). Furthermore, we observe in the coordination and hydrogen bond energies shown in Figure 10d,e, similar to the case of C =0.035, the staged energy variation of coordination interactions and a diminished trend of hydrogen bond interactions in the system with $\varepsilon_c = 25.0\varepsilon$ and 50.0ε , which also fits their structural evolutions, i.e., the variations in the neighbor numbers (Figure S5a,b). Such results also indicate that the sequential breakage of these two kinds of noncovalent networks exists during deformation, and further confirm that the MNs built by low coordination interaction strength cannot exhibit the typical sequential breakage.

To further analyze the poor effects of low ε_c , systems with C = 0.067, ε_c = 10.0 ε and different N_c are studied and the detailed results of their mechanical properties are presented as follows. Figure 11a shows the tensile stress-strain curves for the different number of coordination beads, and the corresponding dissipated work is shown in Figure 11b. Surprisingly, compared with system $N_c = 0$, even the number of coordination beads reaches 150, all compounded systems $(N_c \neq 0)$ show reduced tensile stress and dissipated work during the whole deformation process. Also, different from the results in Figure 4a,b, the number of coordination beads shows less dependence on the stress and dissipated work. According to Figure 11b, it has been observed that the coordination network with low interaction strength ($\varepsilon_c = 10.0\varepsilon$), whose strength is comparable with that of hydrogen bond network ($\varepsilon_{
m h}$ = 5.0ε), fails to toughen the systems efficiently. It can be further confirmed by the comparison in the chain orientation during deformation. As Figure 11c shows, even the values of the chain orientation are very close to each other when strain initiates, later ($\varepsilon_T > 1.5$) the orientation of the system $N_c = 0$ is distinctly higher than that of all of the compounded systems, which further demonstrates that coordination cross-links constructed by $\varepsilon_c = 10.0\varepsilon$ are not strong enough to induce oriented polymer chains so as to sustain the stress. For the energy viewpoint, as Figure 11d,e reveals, the energy of coordination interaction network, together with the hydrogen bond interaction network clearly decreases with the increasing strain, without exhibiting a similar plateau in energy observed in the toughened MNs before, which is also supported by the structural evolutions, i.e., variations in the neighbor numbers (Figure S6a,b). Generally, the total coordination interaction energy is smaller than the total hydrogen bond interaction energy, which indicates an insufficient contribution to the total nonbonded interaction and some damage to both noncovalent networks. Finally, this comparison reveals that not all kinds of coordination interaction can help to toughen the elastomers. In summary, the fragile coordination cross-links constructed by ε_c = 10.0ε are easy to be sacrificed and induce a decrease in the orientation of the polymer chain, thus these less oriented polymer chains fail to sustain the stress. Meanwhile, the sequential breakage of different noncovalent associations is absent for the fragile coordination cross-links.

After revealing the key factors influencing in the toughening effect, i.e., the sufficient and strong coordination cross-links, we need to confirm the toughening effect by the MNs with a high cross-linking density and a strong coordination interaction. In

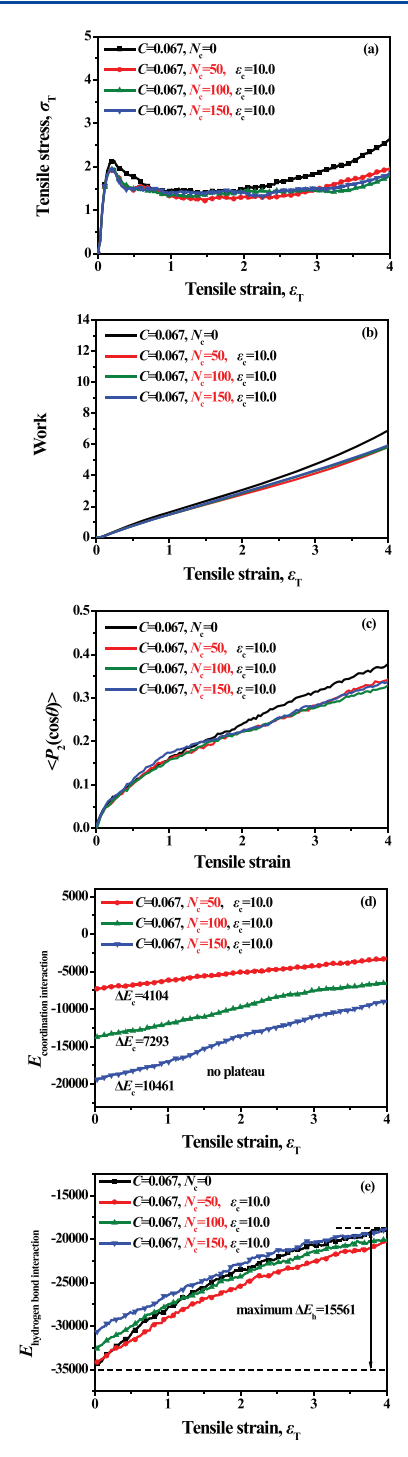


Figure 11. (a) Stress—strain curves for the different number of coordination beads N_c . (b) Dissipated work obtained by integrating the stress—strain curves. (c) Chain orientation of systems corresponding to the stress—strain curves. The total (d) coordination interaction energy and (e) hydrogen bond interaction energy as a function of strain during the tensile process. The ΔE for the coordination interaction and hydrogen bond interaction is calculated by $\Delta E = E(\varepsilon_{\rm T} = 4.0) - E(\varepsilon_{\rm T} = 0)$.

the following comparison, first, we introduce high chemical cross-linking density (C=0.067) to all systems, which will enhance the tensile stress and simultaneously provide enough and effective potential noncovalent cross-linking sites. Then, the strength of the coordination interaction is set to $\varepsilon_c=50.0\varepsilon$ Figure 12a shows the tensile stress–strain curves for the

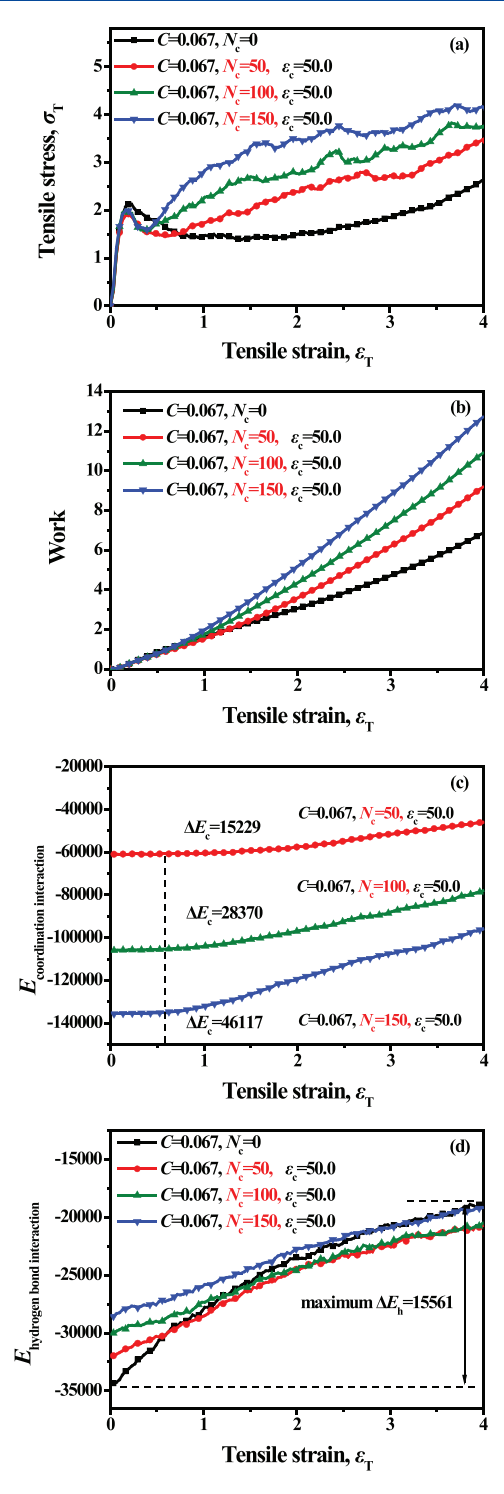


Figure 12. (a) Stress—strain curves for the different number of coordination beads $N_{\rm c}$. (b) Dissipated work obtained by integrating the stress—strain curves. The total (c) coordination interaction energy and (d) hydrogen bond interaction energy as a function of strain during the tensile process. The ΔE for the coordination interaction and hydrogen bond interaction is both calculated by $\Delta E = E(\varepsilon_{\rm T} = 4.0) - E(\varepsilon_{\rm T} = 0)$.

systems with the different number of coordination beads (N_c) . Different from the long stress plateau exhibited by the system with $N_c = 0$, the stress of the MN systems shows a relatively rapid increasing trend after the yielding point as we observed in Figure 10a. It is found that the tensile stress monotonically

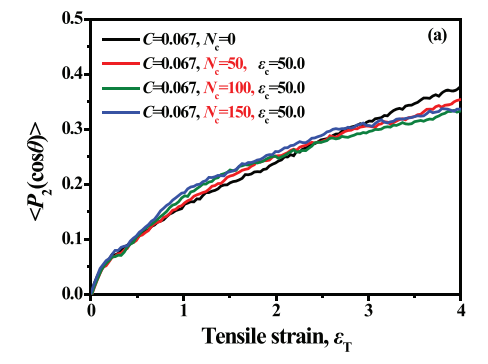
increases with an increase in the number of coordination beads for all compounded systems and all of them show better tensile strength than the system $N_c = 0$ (after yielding point). Also, as expected, the dissipated work demonstrates a prominent toughening effect after we introduce the high-strength coordination interaction network to the systems (Figure 12b).

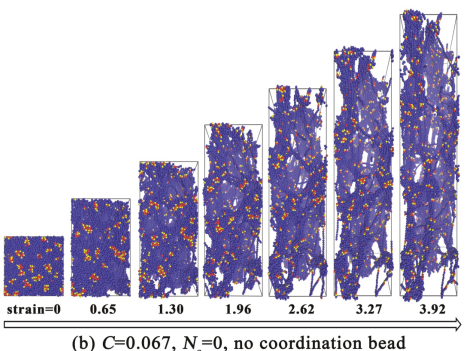
Even though the contribution of the hydrogen bond interaction network has been weakened and partly replaced by the other noncovalent network, all of the systems with coordination beads filled exhibit a typical sequential breakage behavior, which can be clearly seen according to Figure 12c,d. Also, the variations in the neighbor number, i.e., the structural evolutions provide further confirmation for the staged decrease and monotonic decrease in the number of coordination and hydrogen bond cross-links, separately (Figure S7a,b). These observations further confirm the former discussion that introducing coordination bonds with sufficient interaction strength is the key factor in designing the MNs.

However, when we consider the chain orientation during the tensile process (Figure 13a), it is seen that only small enhancements exist in the values of orientation with $N_{\rm c}$ increasing when the strain is smaller than 3.0. As we discussed before, the high cross-linking density will greatly enhance the chain orientation, which screens the chain orientation contributed by the physical cross-linking sites (Figure S4). In addition, as shown in Figure 13b,c, the cavities and voids merge and grow slowly in both the system with $N_{\rm c}=0$ and the system with $N_{\rm c}=150$, and no obvious fracture behavior can be found during deformation.

In the systems with different cross-linking density, we observed different mechanical responses after the strain reaches the yielding point: the stress of the system with C=0.035 shows a deceased trend when the strain is large enough, while that of the systems with C=0.067 never shows a decreased trend for the chain orientation, which is greatly enhanced by the high cross-linking density. The toughening mechanism is concluded according to the following observations:

- (a) In the systems with C = 0.035, the sufficient and strong coordination cross-links induce many long and highly oriented polymer chains/fibrils, which also help prevent the voids and cavitations from growing and propagating quickly (Figures 4, 5 and 8).
- (b) In the systems with C=0.067, introducing the sufficient and strong coordination interaction can also induce an increase in the dissipated work, i.e., the toughness. However, their values of chain orientation are similar to each other because of the enhancement from the high covalent cross-linking density, which finally screens the contribution from the noncovalent cross-links (Figures 10-13). Besides, these results further confirm our conclusion that introducing a coordination interaction with $\varepsilon_c \geq 25.0\varepsilon$ is essential in toughening the MNs. After we observed that the low coordination interaction strength results in the decrease of the chain orientation, we infer that the higher interaction strength will also induce highly oriented polymer chains/fibrils in the systems with C=0.067.
- (c) Even though the observations in the above situations are different, we still conclude that the toughening effect dominantly arises from oriented polymer chains which





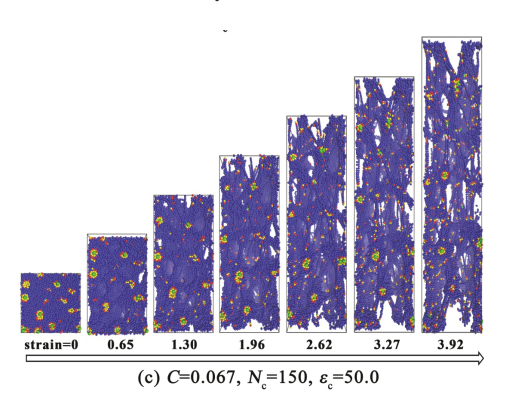


Figure 13. (a) Chain orientation of systems with the different number of coordination beads N_c , which is corresponding to Figure 12a. Snapshots of the systems (b) C = 0.067, $N_c = 0$ and (c) C = 0.067, $N_c = 150$, $\varepsilon_c = 50.0$ showing the deformation state at different strain.

are induced by the sufficient and strong noncovalent coordination cross-links.

4. CONCLUSIONS

In the present study, we build a series of multiple networks (MNs) consisting of the covalently cross-linked network and two kinds of noncovalent networks with different interaction strengths, to explore the effects of the number of coordination beads (N_c) , the coordination interaction strength (ε_c) and the chemical cross-linking density (C) on the toughening mechanism and mechanical behavior. The simulation results reveal that:

(a) In all systems successfully toughened by MNs, which exhibit much more dissipated work than the reference system, the increased chain orientation contributed by the introduced coordination interaction dominantly leads to the strengthened tensile stress and further enhancement of the toughness. The oriented polymer chains/fibrils are seen to prevent the cavitations and

voids from growing and propagating quickly to sustain the external stress, and they are helpful for the breakage of noncovalent associations to dissipate energy. Meanwhile, the absolute value of the nonbonded energy of the coordination interaction and the corresponding neighbor number show a staged decrease trend during deformation, which is totally distinct from those of the hydrogen bond interaction.

- (b) The sequential breakage of different noncovalent associations is characteristic of the MNs. Explicitly, when subjected to an external force, the hydrogen bond network dominantly dissipates the energy when the strain initiates, while the coordination network is not influenced until the strain reaches around 0.6, and then subsequently dissipates the energy to contribute to the toughening of MNs.
- (c) To toughen elastomers by designing the MNs, independent of the cross-linking density, introducing a coordination interaction with $\varepsilon_{\rm c} \geq 25.0\varepsilon$ is of significance in cooperating with the hydrogen bond ($\varepsilon_{\rm h} = 5.0\varepsilon$). Moreover, sufficient coordination cross-links are essential. Compared with the unfilled system, although the yielding stress reduces for the repulsive interaction between coordination beads and polymer chains, the MN elastomer shows a much longer stress plateau (for low cross-linking density) and rapidly increased tensile stress after the yielding point (for high cross-linking density).
- (d) Not all MNs incorporation can successfully toughen the elastomers. Not only will the insufficient coordination cross-links interfere with the toughening effect with the hydrogen bond interaction, but they also cannot induce the polymer chains to be oriented to sustain the stress. In addition, MNs with low coordination interaction strength also shows decreased toughness and the absence of the sequential breakage, resulting from the reduced chain orientation for those fragile coordination cross-links.

In general, this work not only demonstrates the toughening mechanism of the double sacrificial network in MNs under deformation but also provides some guidelines for the fabrication of materials with good mechanical properties via multiple network design.

ASSOCIATED CONTENT

S Supporting Information

The Supporting Information is available free of charge on the ACS Publications website at DOI: 10.1021/acs.macromol.9b00116.

Nomenclature; the glass-transition temperature of MN systems; detailed chemically cross-linking reaction; method to calculate the average number of neighbor beads; the ability of hydrogen bond network to dissipate the energy; the backbone orientation of MNs with different cross-linking densities; the structural evolutions of noncovalent cross-links for different interaction strengths; the structural evolutions of noncovalent cross-links for the different number of coordination beads (low interaction strength); the structural evolutions of noncovalent cross-links for different number of coordination beads (high interaction strength) (PDF)

AUTHOR INFORMATION

Corresponding Authors

*E-mail: liujun@mail.buct.edu.cn (J.L.). *E-mail: venkat@che.utexas.edu (V.G.).

ORCID (

Jun Liu: 0000-0001-7369-1875

Venkat Ganesan: 0000-0003-3899-5843 Liqun Zhang: 0000-0002-8106-4721

Notes

The authors declare no competing financial interest.

ACKNOWLEDGMENTS

We would like to acknowledge the financial support from the Major Program (51790502) and the Major International Cooperation (51320105012) of the National Nature Science Foundation of China, the National Natural Science Foundation of China (51873006, 21674010, and 51333004), the Beijing Natural Science Foundation (2182053) and the National 973 Basic Research Program of China 2015CB654700 (2015CB654704). VG acknowledges generous support by grants from Robert A. Welch Foundation (Grant F1599), and the National Science Foundation (CBET-17069698 and DMR-1721512). The super-calculation center of "Tianhe number two" and the cloud calculation platform of the Beijing University of Chemical Technology (BUCT) are both greatly appreciated.

REFERENCES

- (1) Qin, X.; Han, B.; Lu, J.; Wang, Z.; Sun, Z.; Wang, D.; Russell, T. P.; Zhang, L.; Liu, J. Rational design of advanced elastomer nanocomposites towards extremely energy-saving tires based on macromolecular assembly strategy. *Nano Energy* **2018**, 48, 180–188.
- (2) Deng, F.; Ito, M.; Noguchi, T.; Wang, L.; Ueki, H.; Niihara, K.-i.; Kim, Y. A.; Endo, M.; Zheng, Q.-S. Elucidation of the reinforcing mechanism in carbon nanotube/rubber nanocomposites. *ACS Nano* **2011**, *5*, 3858–3866.
- (3) Wang, W.; Zhao, D.; Yang, J.; Nishi, T.; Ito, K.; Zhao, X.; Zhang, L. Novel slide-ring material/natural rubber composites with high damping property. *Sci. Rep.* **2016**, *6*, No. 22810.
- (4) Frogley, M. D.; Ravich, D.; Wagner, H. D. Mechanical properties of carbon nanoparticle-reinforced elastomers. *Compos. Sci. Technol.* **2003**, *63*, 1647–1654.
- (5) Wang, Z.; Liu, J.; Wu, S.; Wang, W.; Zhang, L. Novel percolation phenomena and mechanism of strengthening elastomers by nanofillers. *Phys. Chem. Chem. Phys.* **2010**, *12*, 3014–3030.
- (6) Domun, N.; Hadavinia, H.; Zhang, T.; Sainsbury, T.; Liaghat, G.; Vahid, S. Improving the fracture toughness and the strength of epoxy using nanomaterials—a review of the current status. *Nanoscale* **2015**, *7*, 10294–10329.
- (7) Johnson, J. A.; Turro, N. J.; Koberstein, J. T.; Mark, J. E. Some hydrogels having novel molecular structures. *Prog. Polym. Sci.* **2010**, 35, 332–337.
- (8) Gong, J. P.; Katsuyama, Y.; Kurokawa, T.; Osada, Y. Doublenetwork hydrogels with extremely high mechanical strength. *Adv. Mater.* **2003**, *15*, 1155–1158.
- (9) Wu, J.; Cai, L.-H.; Weitz, D. A. Tough Self-Healing Elastomers by Molecular Enforced Integration of Covalent and Reversible Networks. *Adv. Mater.* **2017**, *29*, No. 1702616.
- (10) Li, C.-H.; Wang, C.; Keplinger, C.; Zuo, J.-L.; Jin, L.; Sun, Y.; Zheng, P.; Cao, Y.; Lissel, F.; Linder, C.; et al. A highly stretchable autonomous self-healing elastomer. *Nat. Chem.* **2016**, *8*, 618.
- (11) Holten-Andersen, N.; Harrington, M. J.; Birkedal, H.; Lee, B. P.; Messersmith, P. B.; Lee, K. Y. C.; Waite, J. H. pH-induced metalligand cross-links inspired by mussel yield self-healing polymer

networks with near-covalent elastic moduli. *Proc. Natl. Acad. Sci. U.S.A.* **2011**, *108*, 2651–2655.

- (12) Liu, J.; Tan, C. S. Y.; Yu, Z.; Li, N.; Abell, C.; Scherman, O. A. Tough Supramolecular Polymer Networks with Extreme Stretchability and Fast Room-Temperature Self-Healing. *Adv. Mater.* **2017**, *29*, No. 1605325.
- (13) Murphy, E. B.; Wudl, F. The world of smart healable materials. *Prog. Polym. Sci.* **2010**, *35*, 223–251.
- (14) Varley, R. J.; van der Zwaag, S. Towards an understanding of thermally activated self-healing of an ionomer system during ballistic penetration. *Acta Mater.* **2008**, *56*, 5737–5750.
- (15) Chen, Y.; Kushner, A. M.; Williams, G. A.; Guan, Z. Multiphase design of autonomic self-healing thermoplastic elastomers. *Nat. Chem.* **2012**, *4*, 467–472.
- (16) Liu, J.; Liu, J.; Wang, S.; Huang, J.; Wu, S.; Tang, Z.; Guo, B.; Zhang, L. An advanced elastomer with an unprecedented combination of excellent mechanical properties and high self-healing capability. *J. Mater. Chem. A* **2017**, *5*, 25660–25671.
- (17) Cordier, P.; Tournilhac, F.; Soulié-Ziakovic, C.; Leibler, L. Self-healing and thermoreversible rubber from supramolecular assembly. *Nature* **2008**, *451*, 977.
- (18) Chen, Q.; Zhu, L.; Chen, H.; Yan, H.; Huang, L.; Yang, J.; Zheng, J. A Novel Design Strategy for Fully Physically Linked Double Network Hydrogels with Tough, Fatigue Resistant, and Self-Healing Properties. *Adv. Funct. Mater.* **2015**, 25, 1598–1607.
- (19) Ducrot, E.; Chen, Y.; Bulters, M.; Sijbesma, R. P.; Creton, C. Toughening elastomers with sacrificial bonds and watching them break. *Science* **2014**, 344, 186–189.
- (20) Sun, T. L.; Kurokawa, T.; Kuroda, S.; Ihsan, A. B.; Akasaki, T.; Sato, K.; Haque, M. A.; Nakajima, T.; Gong, J. P. Physical hydrogels composed of polyampholytes demonstrate high toughness and viscoelasticity. *Nat. Mater.* **2013**, *12*, 932.
- (21) Sun, J.-Y.; Zhao, X.; Illeperuma, W. R.; Chaudhuri, O.; Oh, K. H.; Mooney, D. J.; Vlassak, J. J.; Suo, Z. Highly stretchable and tough hydrogels. *Nature* **2012**, *489*, 133.
- (22) Liu, J.; Wang, S.; Tang, Z.; Huang, J.; Guo, B.; Huang, G. Bioinspired engineering of two different types of sacrificial bonds into chemically cross-linked cis-1,4-polyisoprene toward a high-performance elastomer. *Macromolecules* **2016**, *49*, 8593–8604.
- (23) Huang, J.; Tang, Z.; Yang, Z.; Guo, B. Bioinspired interface engineering in elastomer/graphene composites by constructing sacrificial metal—ligand bonds. *Macromol. Rapid Commun.* **2016**, 37, 1040—1045.
- (24) Cao, J.; Li, J.; Chen, Y.; Zhang, L.; Zhou, J. Dual Physical Crosslinking Strategy to Construct Moldable Hydrogels with Ultrahigh Strength and Toughness. *Adv. Funct. Mater.* **2018**, 28, No. 1800739.
- (25) Burnworth, M.; Tang, L.; Kumpfer, J. R.; Duncan, A. J.; Beyer, F. L.; Fiore, G. L.; Rowan, S. J.; Weder, C. Optically healable supramolecular polymers. *Nature* **2011**, *472*, 334.
- (26) Yuan, J.; Zhang, H.; Hong, G.; Chen, Y.; Chen, G.; Xu, Y.; Weng, W. Using metal—ligand interactions to access biomimetic supramolecular polymers with adaptive and superb mechanical properties. *J. Mater. Chem. B* **2013**, *1*, 4809–4818.
- (27) Tang, Z.; Huang, J.; Guo, B.; Zhang, L.; Liu, F. Bioinspired engineering of sacrificial metal–ligand bonds into elastomers with supramechanical performance and adaptive recovery. *Macromolecules* **2016**, *49*, 1781–1789.
- (28) Zhang, X.; Liu, J.; Zhang, Z.; Wu, S.; Tang, Z.; Guo, B.; Zhang, L. Toughening Elastomers Using a Mussel-Inspired Multiphase Design. ACS App. Mater. Interfaces 2018, 10, 23485–23489.
- (29) Zhang, Z.; Liu, J.; Zhang, L. Tuning the structure and mechanical properties of double-network elastomer: Molecular dynamics simulation (in Chinese). *Chin. Sci. Bull.* **2018**, 63, 3631–3641
- (30) Gong, J. P. Why are double network hydrogels so tough? *Soft Matter* **2010**, *6*, 2583–2590.

(31) Kremer, K.; Grest, G. S. Dynamics of entangled linear polymer melts: A molecular-dynamics simulation. *J. Chem. Phys.* **1990**, *92*, 5057–5086.

- (32) Sen, S.; Kumar, S. K.; Keblinski, P. Viscoelastic properties of polymer melts from equilibrium molecular dynamics simulations. *Macromolecules* **2005**, *38*, 650–653.
- (33) Bennemann, C.; Paul, W.; Baschnagel, J.; Binder, K. Investigating the influence of different thermodynamic paths on the structural relaxation in a glass-forming polymer melt. *J. Phys.: Condens. Matter* **1999**, *11*, 2179.
- (34) Perrin, C. L.; Nielson, J. B. "Strong" hydrogen bonds in chemistry and biology. *Annu. Rev. Phys. Chem.* **1997**, 48, 511–544.
- (35) Liu, W.; Thorp, H. H. Bond valence sum analysis of metalligand bond lengths in metalloenzymes and model complexes. 2. Refined distances and other enzymes. *Inorg. Chem.* **1993**, 32, 4102–4105.
- (36) Steiner, T. Unrolling the hydrogen bond properties of C-H··· O interactions. *Chem. Commun.* **1997**, 727–734.
- (37) Desiraju, G. R. The CH. cntdot.. cntdot.. cntdot. O hydrogen bond in crystals: what is it? *Acc. Chem. Res.* **1991**, *24*, 290–296.
- (38) Uddin, J.; Frenking, G. Energy Analysis of Metal-Ligand Bonding in Transition Metal Complexes with Terminal Group-13 Diyl Ligands (CO) 4Fe-ER, Fe (EMe) 5 and Ni (EMe) 4 (E=B-Tl; R=Cp, N (SiH3) 2, Ph, Me) Reveals Significant π Bonding in Homoleptical Molecules. *J. Am. Chem. Soc.* **2001**, *123*, 1683–1693.
- (39) Steiner, T. The hydrogen bond in the solid state. *Angew. Chem., Int. Ed.* **2002**, 41, 48–76.
- (40) Chen, Y.; Liu, L.; Yang, Q.; Wen, S.; Zhang, L.; Zhong, C. Computational study of nanoparticle dispersion and spatial distribution in polymer matrix under oscillatory shear flow. *Langmuir* **2013**, *29*, 13932–13942.
- (41) Allen, M. P.; Tildesley, D. J. Computer Simulation of Liquids; Oxford University Press: New York, 2017.
- (42) Binder, K.; Baschnagel, J.; Paul, W. Glass transition of polymer melts: test of theoretical concepts by computer simulation. *Prog. Polym. Sci.* **2003**, *28*, 115–172.
- (43) Liu, J.; Wu, S.; Cao, D.; Zhang, L. Effects of pressure on structure and dynamics of model elastomers: A molecular dynamics study. *J. Chem. Phys.* **2008**, *129*, No. 154905.
- (44) Kroll, D.; Croll, S. Influence of crosslinking functionality, temperature and conversion on heterogeneities in polymer networks. *Polymer* **2015**, *79*, 82–90.
- (45) Zheng, Z.; Xia, X.; Zeng, X.; Li, X.; Wu, Y.; Liu, J.; Zhang, L. Theoretical Model of Time—Temperature Superposition Principle of the Self-Healing Kinetics of Supramolecular Polymer Nanocomposites. *Macromol. Rapid Commun.* **2018**, *39*, No. 1800382.
- (46) Gao, Y.; Liu, J.; Shen, J.; Cao, D.; Zhang, L. Molecular dynamics simulation of the rupture mechanism in nanorod filled polymer nanocomposites. *Phys. Chem. Chem. Phys.* **2014**, *16*, 18483—18492.
- (47) Liu, J.; Shen, J.; Zheng, Z.; Wu, Y.; Zhang, L. Revealing the toughening mechanism of graphene–polymer nanocomposite through molecular dynamics simulation. *Nanotechnology* **2015**, *26*, No. 291003.
- (48) Elder, R. M.; Long, T. R.; Bain, E. D.; Lenhart, J. L.; Sirk, T. W. Mechanics and nanovoid nucleation dynamics: effects of polar functionality in glassy polymer networks. *Soft Matter* **2018**, *14*, 8895–8911.
- (49) Gersappe, D. Molecular mechanisms of failure in polymer nanocomposites. *Phys. Rev. Lett.* **2002**, *89*, No. 058301.
- (50) Meng, D.; Kumar, S. K.; Ge, T.; Robbins, M. O.; Grest, G. S. Crazing of nanocomposites with polymer-tethered nanoparticles. *J. Chem. Phys.* **2016**, *145*, No. 094902.
- (51) Rottler, J.; Barsky, S.; Robbins, M. O. Cracks and crazes: on calculating the macroscopic fracture energy of glassy polymers from molecular simulations. *Phys. Rev. Lett.* **2002**, *89*, No. 148304.
- (52) Gao, J.; Weiner, J. Anisotropy effects on chain-chain interactions in stretched rubber. *Macromolecules* **1991**, *24*, 1519–1525.

(53) Gao, J.; Weiner, J. Simulated polymer melt stress relaxation. I. Plateau behavior. *J. Chem. Phys.* **1995**, *103*, 1614–1620.

- (54) Li, Y.; Kröger, M.; Liu, W. K. Nanoparticle geometrical effect on structure, dynamics and anisotropic viscosity of polyethylene nanocomposites. *Macromolecules* **2012**, *45*, 2099–2112.
- (55) Plimpton, S. Fast parallel algorithms for short-range molecular dynamics. *J. Comput. Phys.* **1995**, *117*, 1–19.
- (56) Liu, J.; Lu, Y. L.; Tian, M.; Li, F.; Shen, J.; Gao, Y.; Zhang, L. The interesting influence of nanosprings on the viscoelasticity of elastomeric polymer materials: Simulation and experiment. *Adv. Funct. Mater.* **2013**, 23, 1156–1163.
- (57) Liu, J.; Shen, J.; Gao, Y.; Zhou, H.; Wu, Y.; Zhang, L. Detailed simulation of the role of functionalized polymer chains on the structural, dynamic and mechanical properties of polymer nanocomposites. *Soft Matter* **2014**, *10*, 8971–8984.
- (58) Liu, J.; Zheng, Z.; Li, F.; Lei, W.; Gao, Y.; Wu, Y.; Zhang, L.; Wang, Z. L. Nanoparticle chemically end-linking elastomer network with super-low hysteresis loss for fuel-saving automobile. *Nano Energy* **2016**, 28, 87–96.
- (59) Liu, J.; Gao, Y.; Cao, D.; Zhang, L.; Guo, Z. Nanoparticle dispersion and aggregation in polymer nanocomposites: insights from molecular dynamics simulation. *Langmuir* **2011**, *27*, 7926–7933.